International Journal of Engineering Research and Science & Technology

IJERST

ISSN : 2319-5991

www.ijerst.com

Email: editor@ijerst.com or editor.ijerst@gmail.com

ISSN 2319-5991 www.ijerst.com

Vol. 14, Issue 4, 2018

EXPLORING THE APPLICATION OF FREQUENCY-DOMAIN CORRELATION TECHNIQUE IN DETECTING IMPACT DAMAGE AND ASSESSING DYNAMIC RESPONSES OF RC BRIDGE PIERS

[1]Dr. VEERAVALLI SITARAM PRASAD ,[2]VENGALA UPENDER,
[3]BOMMU SATISH REDDY, [4]A.PRASHANTH
[1]Professor,[23]Assistant Professor,[4]Student
Department Of Mechanical Engineering
Abdul Kalam Institute of Technological Sciences, Kothagudem, Telangana

ABSTRACT:
In order to improve damage detection in reinforced concrete columns, we looked at the possible uses of damage correlation indices, which are frequency-domain based correlation approaches. Four scaled-down reinforced concrete pier components were struck by researchers using a novel ultra-high drop hammer experiment technique, which simulated the effects of medium-sized autos striking bridge piers. Using an acceleration acquisition device, the members' frequency response functions were evaluated both before and after the injury. The experiments showed that the damage levels of the piers were accurately estimated by the damage correlation indexes (DCI) that considered the multi-order modal frequencies. Additionally, using the commercial application LS-DYNA, an impact finite element model and a modal analysis technique were constructed and matched with the experiments. By aligning the finite element parameters with the experimental data, the impact processes between medium-sized vehicles and reinforced concrete piers were simulated. A peak impact force (PIF) calculation based on damage indices was supplied for vehicle collision situations to ensure that structural design criteria are met.

Key words: Damage detection, numerical models, lateral impacts, reinforced concrete piers, and modal frequencies.

I.INTRODUCTION

The gradual acceleration of the urbanization process had led to rapid growth in the number of vehicles and traffic facilities in the region. Consequently, collisions between vehicles and bridge piers have become the main threat to the safety of urban overpasses. In recent years, researchers have conducted many statistical studies regarding major accidents caused by bridge collapses since the 21st century, among which the accidents involving ships or vehicles impacting bridges were determined to account for approximately 20%.1 In such cases, applications of structural health detection technology are of particular importance. Damage assessments and repair processes require huge economic investment, which may cause difficulties to the implementation of the necessary actions. In fact, the progress which has been made sensor and computer technology has provided improved solution choices for damage assessments. Among the newly introduced technologies, vibration based monitoring methods enable engineers to collect data in real time, allowing structures to be evaluated in real time by comparing the parameters of the original structure with those of the damage state.2 The most commonly used data include natural frequencies3, modal shapes4, mass values5, stiff- ness values6, damping matrixes7, and frequency response functions (FRFs).8

In order to solve the impact problems, various coun- tries have actively put forward corresponding design codes. The most representative code is the proposed AASHTO LRFD,9 which takes the equivalent static force

ISSN 2319-5991 www.ijerst.com

Vol. 14, Issue 4, 2018

of 2670 KN as the design value of bridge piers at a distance of 1500 mm from the road edge. The initial rough finite element model established by Chen et al.10 was used to evaluate its reasonability, and the results showed that the values taken in the aforementioned code were too conservative in some cases. Consequently, the finite element model proposed by Abdelkarim and ElGawady11 was used to verify the above-mentioned values and compare them with those obtained using a 25 ms average peak force method and the equivalent static force calculation method (equation (1)) proposed by Euro-code.12 The results indicated that it was more reasonable to use the average force of the 25 ms peak force proposed by Buth et al.13 as the equivalent static force for structural designs:

$$\mathrm{ESF} = \frac{m v_r^2}{2(\delta_C + \delta_D)} \qquad (1)$$

where m is the mass of the vehicle; Vr denotes the velo-city of the vehicle; dc represents the distance variable between the vehicle head and the center of mass; and dD is the transverse deformation of the column at the impact point. Buth et al.14 used a 36t tractor-semitrailer to carry out transverse impact experiments on a full- scale rigid pier model. The model visually showed the vehicle head crushing, cargo-pier impact, and other mechanical behaviors of the bridge pier. Chen et al.15 constructed an anti-collision guardrail composed of five short columns, and utilized a Dongfeng-EQ140 medium-sized truck to carry out transverse impact experiments. The impact force, deflection, and other parameters were recorded during the experimental pro- cesses. Then, based on the acquired experimental data, a simplified finite element guardrail model was pro- posed. Cai et al.16 carried out impact experiments on 15 square scale columns using a transverse impact experi- mental device. The influencing effects of the slenderness ratios on the impact energy, peak impact force, and member deformations were the main focus in the aforementioned study. In another related study, Zhou et al.17 explored the dynamic responses of concrete pier members under cumulative impact conditions using an ultra-high drop-hammer experimental system. The results showed that with the increases in the damage degrees, the internal energy dissipation capacities of the structures had gradually decreased, and a damage judg- ment method based on the changes in modal frequency was proposed. There is no doubt that previously con- ducted impact experiments have greatly promoted the development of numerical simulations in this field. Adhikary et al.18 carried out weight reduction experi- ments on reinforced concrete beams and established a detailed finite element model to analyze the impact mass ratios, longitudinal reinforcement ratios, concrete compressive strength, and other parameters in detail. In addition, since the dynamic behaviors of beams are more easily observed during impact processes, Pham and Hao19 established a simplified mechanical model and a numerical model of reinforced concrete beams; proposed a method to deduce shear and bending moment diagrams; and confirmed the assumption of the linear inertial force distributions along beams. Also, Chen et al.20 developed an equivalent impact frame for the purpose of simulating the impact effects of large trucks and reinforced concrete columns. Then, by com- paring the deformations and internal energy relation- ships between frames and actual trucks, the equivalence values between the frames and actual trucks were rea- lized. Finally, an appropriate finite element simulation was established in order to verify the overall similarities between them. Sharma et al.21 developed finite element pier models under different vehicle impact conditions and proposed the concept of performance-based design for impact problems. In addition, the damages under different states were successfully classified, and a set of program frameworks was established in order to estimate the capacities and demands of dynamic shear force in RC columns. However, the classification of bridge pier safety grades based on performance design criteria is too vague, and there is no reasonable and reliable quantitative index. In the study, a high-

ISSN 2319-5991 www.ijerst.com

Vol. 14, Issue 4, 2018

applicability calculation method for damage evaluation indexes and impact forces was proposed. In this study's experiments, simplified impact tests using trucks were carried out on circular section piers with a reduced scale. The dynamic responses of the RC columns during impact and the modal frequency changes after damages to the members were measured. Then, in accordance with the experimental results, a detailed finite element model was established, and LS-DYNA software22 was used to verify the experimental results. A finite element model of a fullscale pier under impact conditions was also developed. The results of this study's numerical simulations revealed the relationships between the peak impact

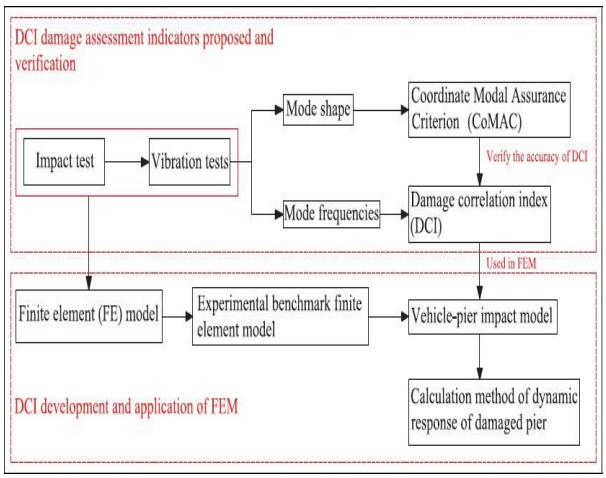

Figure 1. Technical route diagram of the experiments.

force (PIF) and the damage degrees. Then, an equiva- lent static force calculation formula of vehicle impacts in a short period of time was established with the dam- age of the bridge pier considered, which could poten- tially provide valuable references for future structural designs. The research methods involved in this article are shown in Figure 1.

Damage assessment methods based on frequency domains

The basis of the vibration-based impact damage assessment method relies on the change of dynamic response caused by the existence of damage. This phenomenon makes it possible to identify the existence of damage from the change of dynamic response. In this section, two types of damage indicators are introduced. The one is the Modal Assurance Criterion (MAC)23 and the Coordinate Modal Assurance Criterion (CoMAC).24 This indicator is used to express the deviation of the mode shape before and after the damage of the reinforced concrete structure. The difference is because MAC only considers the deviation of the first-order mode shape, COMAC considers the deviation of the multi-order mode shape. The second is the damage correlation coefficient (DCI), which can reflect the difference of multi-mode frequencies before and after structural damage. In this research, CoMAC is considered as a traditional damage assessment index, and the damage index DCI proposed for impact damage is the object to be verified.

2. MAC and CoMAC

The MAC is a dimensionless scalar constant, which represents the degree of correlation between the modal vector and another reference modal vector, as shown in equation (2). In the equation, CAi represents the i-order modal vector from State A. The co-ordinate modal assurance criterion (COMAC)24 is an extension of the modal assurance criterion (MAC), and its correlation is modal related. As shown in equation (3), CAij is the j- order mode shape at point i in State A:

$$\mathrm{MAC}(\{\psi_{\mathrm{A}i}\},\{\psi_{\mathrm{B}j}\}) = \frac{\left|\{\psi_{\mathrm{A}i}\}\{\psi_{\mathrm{B}j}\}\right|^2}{\left(\{\psi_{\mathrm{A}i}\}^t\{\psi_{\mathrm{A}i}\}\right)\left(\{\psi_{\mathrm{B}j}\}^t\{\psi_{\mathrm{B}j}\}\right)} \quad (2)$$

$$\mathrm{COMAC}(\{\psi_{\mathrm{A}ij}\},\{\psi_{\mathrm{B}ij}\}) = \frac{\sum_{j=1}^{N}\left|\{\psi_{\mathrm{A}ij}\}\{\psi_{\mathrm{B}ij}\}\right|^2}{\sum_{j=1}^{N}\{\psi_{\mathrm{A}ij}\}^2\sum_{j=1}^{N}\{\psi_{\mathrm{B}ij}\}^2} \quad (3)$$

Damage correlation index (DCI)

In this study, the damage degrees were evaluated by the differences or similarities between the original modal frequency and the damage modal frequency. The quantitative value was used to evaluate the differences between the two samples. The sample Pearson Correlation

ISSN 2319-5991 www.ijerst.com

Vol. 14, Issue 4, 2018

Coefficient (PCC)25 in the form of a covariance was applicable to the problem. As shown in equation (4), A and B, respectively, represent the two states of health and damaged, Ai represents the i-th order modal frequency in the structural health state. A is the mean value of the frequency sample in the healthy state, and S_A is the standard deviation within the sample of this state:

$$PCC_{A,B} = \frac{\sum_{i=1}^{n}(A_i - \overline{A})(B_i - \overline{B})}{(n-1)\sigma_A \sigma_B} \quad (4)$$

$$\overline{A} = \frac{1}{n}\sum_{i=1}^{n} A_i \quad (5)$$

$$\sigma_A = \sqrt{\frac{1}{n-1}\sum_{i=1}^{n}(A_i - \overline{A})^2} \quad (6)$$

For real numbers with PCC value of [21,1], 1 repre- sents the linear correlation; 0 represents the complete correlation; and 21 represents the reverse or indirect correlation between the data sets compared. However, such cases do not appear in this study since they repre- sent the reverse correlation of the frequency. Therefore, assuming that PCC is bounded in the range of [0, 1], the damage correlation coefficient DCI could be calculated. It was not difficult to determine that the value of DCI was 0 when the column was undamaged and 1 when the correlation was completely lost:

$$DCI = 1 - |PCC_{A,B}| \in R \quad (7)$$

Experimental processes and analysis results

This object is to study the impact of the effective loss characteristic index, were divided into two steps, first by a lateral member percussive impact system, and then the member after injury vibration test, measured modal parameters. For this study, four circular cross-section 1:3 scaled bridge pier components are designed. The specific dimensions of the bridge pier model are given in Section ‘‘Vehicle-bridge impact model,’’ and the test model is scaled based on the p theory proposed by Buckingham. In the process of pouring, ensure that the materials used for the scaled components and the full-scale bridge piers are the same. At this time, the scale effect of the material properties is 1:1:

3. Experimental processes

Preparation of the damaged components. The detailed spe- cimens are shown in Figure 2. Each specimen consisted of a 900 3 300 3 400 mm3 RC base and a circular RC column with a section radius of 170 mm and a height of 2200 mm. All of the specimens were cast using concrete with a cube compressive strength of 42 MPa.

The impact testing instrument was a super-high heavy- duty drop-hammer experimental testing machine system, which was composed of a vertical drop-hammer driving system and a horizontal impact system (Figure 3). As shown in Figure 3(a), the kinetic energy of the horizontal impact test vehicle was provided by the vertical drop- hammer driving system. The conversion relationship is shown in equation (8), where m1 and m2 represent the steel impactor mass and the drop weight mass, g is the

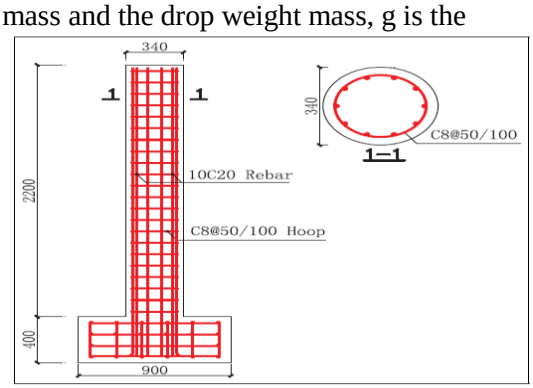

Figure 2. Specimen dimensions and detailed.

acceleration of gravity, h represents the release height of the drop weight, and m is the track dynamic friction coefficient. Table 1 details the basic information of the experimental components and the impacting scheme. The impact of the damage degree on the dynamic response of the column is reflected by the cumulative impact:

$$0.5 \times (m_1 + m_2)v_0^2 + \mu m_1 g = m_2 g h \quad (8)$$

Vibration tests. This study’s modal tests were carried out on the damaged components after impact. Uninstall axial load in order to ensure

ISSN 2319-5991 www.ijerst.com

Vol. 14, Issue 4, 2018

the axial force is not involved in the test, and the upper portion of the col- umn is maintained free vibration. Vibration testing system shown in Figure 4(a) and (b), 10 accelerometers were distributed in the direction of impact specimen back (Figure 4) to ensure that the measured third-order modes. Externally stimulated the front of the impact until the column frequency measurement results are stable. Wherein the accelerometers was used to measure the vibration characteristics of the pier during excita- tion, then the data transmitted to the data logger, the last time domain signal was collected by the computer and obtain a frequency domain data by Fast Fourier Transform. Figure 4(c) shows the acceleration time-domain data collected by the damaged column C1. It is not difficult to observe that the frequency of each order of the damaged column decreases, especially at the higher order frequencies. The appropriate number of accelerometers to ensure the accuracy of the experiment.

Table 1. Information of the components

Specimen	Longitudinal reinforcement ratio ρ_0 (%)	Hoop reinforcement ratio ρ_s (%)	Impact velocity at first-second-, third loading (V_1–V_2–V_3) (m/s)	Axial compression ratio ρ_a (%)
C1	10C20 (2.7)	8@50 (1.7)	4.5	30
C2			4.5–4.5–4.5	20
C3		8@100 (0.9)	4.5–4.5	20
C4		8@150 (0.5)	4.5	20

The axial compression ratio is calculated by $\rho_a = f_{axial}/(\pi r^2 f_c + A_s f_y)$.

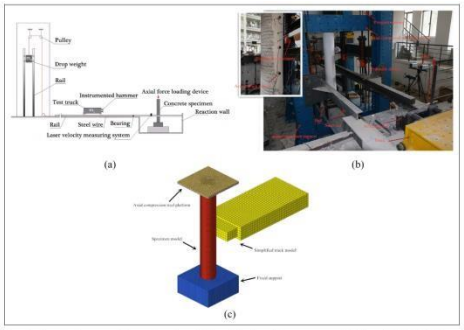

Figure 3. Impact testing system: (a) experimental test 2D view, (b) horizontal impact system, and (c) FE model of the RC column with the steel impactor.

Stiffness measurements. It is necessary to measure the change in the overall stiffness of the column, but the shear stiffness and bending stiffness cannot be made in detail to distinguish during the experiment, the stiffness variation will be described using the overall stiffness of the column in this study. Following impact, the axial pressure was unloaded in order to ensure that the upper rigid plate was no longer in contact with the column. Equal increment transverse force (100 kn, 200 kn, and 300 kn) was applied to the top of the column using the reaction wall. The magnitude of the force was recorded by a dynamometer, and the displacement changes were recorded using a displacement meter installed on the top of the column, as shown in Figure 5, in which Dd represents the displacement differences. Equation (9) was used as the calculation formula of the column stiff- ness, E is the modulus of elasticity, and I is the moment of inertia of the section.

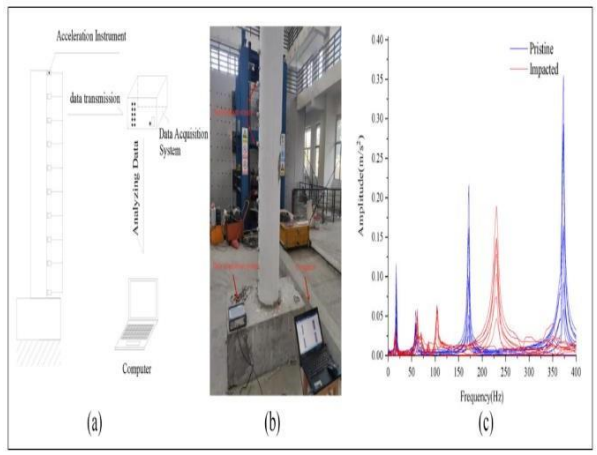

Figure 4. Modal testing system: (a) analytic flowcharts, (b) experimental facility, and (c) comparison of frequency response plots of post-impact and original RC piers.

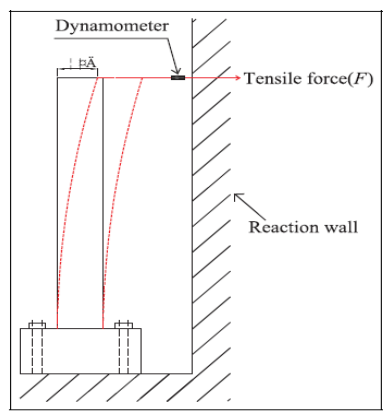

Figure 5. Stiffness measurement system.

$$K = \frac{3EI}{l^3} = \Delta F / \Delta\delta \qquad (9)$$

International Journal of Engineering Research and Science & Technology

ISSN 2319-5991 www.ijerst.com

Vol. 14, Issue 4, 2018

4. Experimental results and analysis

Modal experiments. Figure 6 and Table 2 detail this study's comparison of the results of the experimental identifications of the natural frequencies. It was found that the cumulative impacts resulted in decreased stiff- ness of the sections where cracking occurred. The decreases in the natural frequencies caused by the development of cracks were not monotonic.26 When the damage was small, the change of the first-order fre- quency was not sensitive, and the degree of damage cannot be characterized. The DCI calculation results showed that this index was extremely sensitive to damage due to the consideration of multi-order modal frequencies. The DCI will increase as the degree of damage increases, contrary to the development trend of CoMAC. Compared to using only the first-order modal frequency, it is more reasonable to use DCI as an evaluation indicator.

Similarly, the changes in the modal shapes could not be ignored. Table 3 shows the modal shape measure- ment results of Component C2 before and after impact. The first-order mode shape was not sensitive to the changes in the damage degrees. However, by observing the change processes of the second-order and third- order mode shapes, it could be preliminarily judged that the damage locations. The cracks were dense at this location, which proves the effectiveness of the method.

Impact experiments. Figure 7 shows the relationships between the time history changes and the damage degrees of the three impact forces of component C2. As the degree of column damage increases, the column DCI increases and the peak impact force (PIF) decreases. The smaller losses in the stiffness values were found to have little effect on the peak impact force. However, the pier responses were noticeably weakened after two impacts. The lack of column stiffness resulted in the weakening of the responses.

Stiffness verification. The changes in the values of the stiffness of the components before and after impact were obtained using the method described in Section ''Stiffness measurement.''Table 4 details the statistics of the change rates of the stiffness values of all the components.

The decreases in the overall structural stiffness caused by the impacts resulted in changes in a series of natural frequencies. The development of this problem

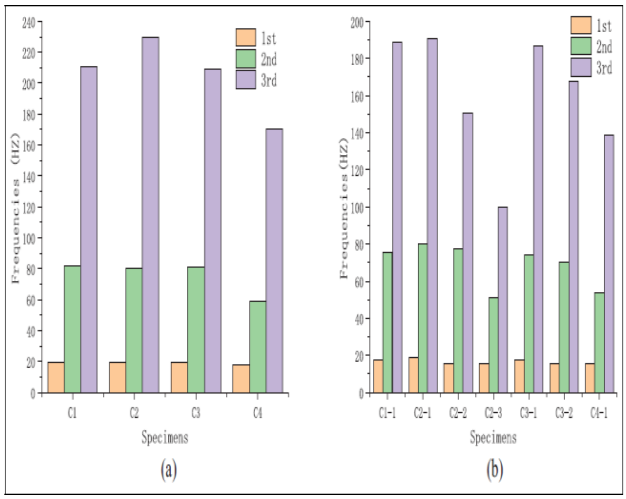

Figure 6. Modal frequencies of the components: (a) modal frequencies (undamaged) and (b) modal frequencies (damaged).

Table 2. Modal test results

Specimens	Experimental			FEM			CoMAC	DCI
	Frequencies	DIFF (%)	Stiffness change (%)	FEM-PRED	Frequencies	DIFF (%)		
C1								
Undamaged			0	0		2.82	1	0
1st-order	19.53				18.98	10.29		
2nd-order	82.03				90.46	2.63		
3rd-order	210.99				205.44			
Impact-1			50.62	0.16		2.54	0.971	0.0001
1	17.57	−9.99			17.13	2.90		
2	75.70	−7.71			73.51	4.24		
3	188.95	−10.44			180.94			
C2								
Undamaged			0	0		2.82	1	0
1	19.53				18.98	12.74		
2	80.24				90.46	10.48		
3	229.49				205.44			
Impact-1			49.77	0.18		10.22	0.984	0.00255
1	19.08	−2.29			17.13	7.87		
2	79.79	−0.56			73.51	5.13		
3	190.73	−16.89			180.94			
Impact-2			68.29	0.23		2.68	0.966	0.01037
1	15.74	−19.36			15.32	2.80		
2	77.71	−3.15			75.53	6.66		
3	150.36	−34.48			140.35			
Impact-3			79.43	0.47		14.68	0.931	0.01858
1	15.74	−19.36			13.43	0.31		
2	50.78	−36.72			50.93	5.86		
3	99.60	−56.60			93.76			
C3								
Undamaged				0		1.21	1	0
1	19.21				18.98	2.80		
2	81.21				83.48	6.74		
3	208.73				194.67			
Impact-1			36.04	0.12		2.10	0.977	0.00005
1	17.58	−8.46			17.21	0.96		
2	74.30	−8.50			73.59	4.64		
3	186.31	−10.72			177.67			
Impact-2			46.92	0.33		3.80	0.963	0.00068
1	15.62	−18.67			15.03	2.25		
2	70.31	−13.42			71.89	2.61		
3	167.47	−19.76			171.85			

Table 2. (Continued)

Specimens	Experimental			FEM			CoMAC	DCI
	Frequencies	DIFF (%)	Stiffness change (%)	FEM-PRED	Frequencies	DIFF (%)		
C4								
Undamaged				0		2.29	1	0
1	17.57				17.98	30.51		
2	58.59				76.47	10.32		
3	169.99				187.53			
Impact-1			78.48	0.19		9.66	0.971	0.00094
1	15.48	−11.91			13.98	14.73		
2	53.54	−8.61			61.43	10.85		
3	138.67	−18.42			153.71	2.82		

The DIFF: under the Experimental describes the initial frequency of the column and the frequency change after column damage; the DIFF: in the FEM describes the difference between the finite element calculation results and the experimental results.

ISSN 2319-5991 www.ijerst.com

Vol. 14, Issue 4, 2018

Table 3. Comparison of the modal shapes of component C2.

Specimens	Mode shapes-undamaged	Mode shapes-damaged
C2-1	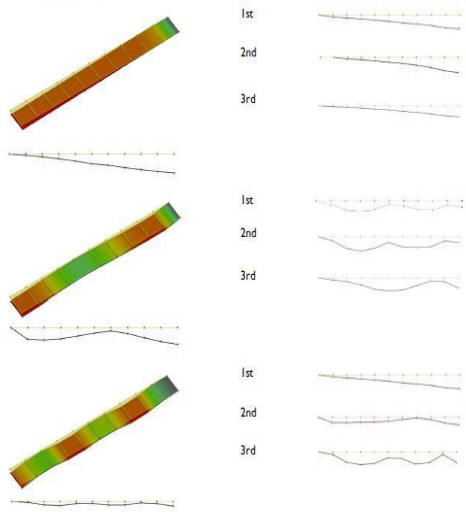	1st 2nd 3rd
C2-2		1st 2nd 3rd
C2-3		1st 2nd 3rd

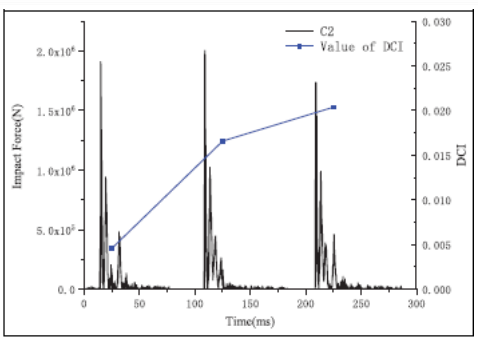

Figure 7. Comparison of the impact force time history and DCI changes of Component C2.

Table 4. Changes in the stiffness.

Specimen	Stiffness *K* (kn/m)	Change ratio (%)
C1		
Undamaged	8052.3	
C1-1	3976.4	50.62
C2		
Undamaged	7436.2	
C2-1	3734.8	49.77
C2-2	2357.7	68.29
C2-3	1529.6	79.43
C3		
Undamaged	6555.8	
C3-1	4192.8	36.04
C3-2	3479.6	46.92
C4		
Undamaged	6713.3	
C4-1	1444.6	78.48

mainly originated from the characteristic value problem of the system vibration equation. Therefore, motion equation (10) of the undamped mechanical system was applied. The first third order frequency approximation of the experimental model was solved using the Rayleigh Method27 and the accuracy of the experimen- tal data was successfully verified. Therefore, in accor- dance with the principle of energy conservation, in which the strain energy at the maximum displacement time is equal to the initial kinetic energy, equation (11) was established.

$$\frac{\partial^2}{\partial x^2}\left[EI(x)\frac{\partial^2 v(x,t)}{\partial x^2}\right] + m(x)\frac{\partial^2 v(x,t)}{\partial t^2} = p(x,t) \qquad (10)$$

$$U_{max} = W_{max} \qquad (11)$$

The strain energy expression of a cantilever beam con- sidering only the displacement in one direction is as follows:

$$W_{max} = \frac{1}{2}\int_0^l EI\left(\frac{\partial^2 y}{\partial x^2}\right)^2 dx \qquad (12)$$

The kinetic energy expression is as follows:

$$U_{max} = \frac{1}{2}\omega^2\int_0^l my^2(x)dx \qquad (13)$$

Therefore, according to equations (10)–(13), the follow- ing was obtained:

$$\omega^2 = \frac{\int_0^l EI\left(\frac{\partial^2 y}{\partial x^2}\right)^2 dx}{\int_0^l my^2(x)dx} \qquad (14)$$

In the current study, based on the above- mentioned method, the natural vibration frequencies of the cantile- ver components under the effects of gravity were solved and the first three order approximate solutions were determined as follows:

$$\omega_1 = \frac{3.5160}{l^2}\sqrt{\frac{EI}{m}}\omega_2 = \frac{22.0345}{l^2}\sqrt{\frac{EI}{m}}\omega_1 = \frac{61.6972}{l^2}\sqrt{\frac{EI}{m}} \qquad (15)$$

The expressions of the structural stiffness were deter- mined (equation (16)), and the structural stiffness were C3 obtained using the calculations detailed in Table 4:

$$K = \frac{3EI}{l^3} \Rightarrow EI = \frac{Kl^3}{3} \qquad (16)$$

In the present research investigation, by comparing the experimental results with the theoretical calculation results, the accuracy levels of the experiments were veri- fied. It was not difficult to determine through the find- ings of the experiments that the low-order frequencies were insensitive to the stiffness degradation phenom- enon. This had led to deviations in the measured values from the

ISSN 2319-5991 www.ijerst.com

Vol. 14, Issue 4, 2018

theoretical approximate solutions. Since this study's experimental processes could not ensure stable fixed boundaries, elastic treatments of the boundaries will be required in order to achieve more accurate calcu- lations. However, the experimental results showed that there were reasonable correlations between the DCI and stiffness changes (Figure 8). Therefore, it was con- sidered that in engineering practices, the measured com- ponent frequency changes could be used to accurately predict the degrees of stiffness loss.

Table 5. Comparison of the theoretical calculations and the experimental data.

Specimens	Frequencies (HZ)								
	1st			2rd			3nd		
	Theo	Exp	Error (%)	Theo	Exp	Error (%)	Theo	Exp	Error (%)
C1	13.30	19.531	31.903	83.38	82.031	−1.645	233.46	210.993	−10.648
C1-1	9.35	17.578	46.809	58.59	75.703	22.605	164.06	188.953	13.174
C2	12.79	19.531	34.514	80.12	80.242	0.152	224.35	229.492	2.241
C2-1	9.06	19.083	52.523	56.78	79.791	28.839	159.00	190.736	16.639
C2-2	7.20	15.749	54.283	45.12	77.717	41.943	126.33	150.365	15.984
C2-3	5.80	15.749	63.172	36.34	50.781	28.438	101.75	99.609	−2.149
C3	12.00	19.213	37.542	75.23	81.212	7.366	210.65	208.73	−0.920
C3-1	9.60	17.588	45.417	60.16	74.304	19.035	168.47	186.314	9.577
C3-2	8.75	15.625	44.000	54.81	70.313	22.049	153.47	167.476	8.363
C4	12.15	17.578	30.880	76.13	58.594	−29.928	213.17	169.992	−25.400
C4-1	5.64	15.484	63.575	35.32	53.547	34.039	98.89	138.672	28.688

In the table, C2-1 represents the experimental data of the C2 member following the first impact; Test represents the experimental result.

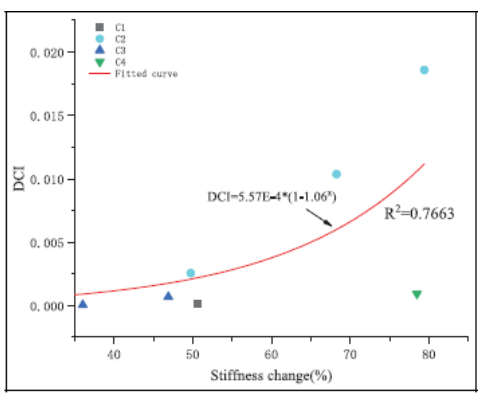

Figure 8. Correlations between the DCI and stiffness losses.

Numerical simulation and discussion

A finite element model which matched with the experi- ments was established using LS-DYNA commercial software. After analysis of the collision by explicit anal- ysis, modal analysis by its implicit analysis. This section calibrates the finite element model and describes the solution to the conversion between algorithms.

Finite element (FE) model

The adopted 3D nonlinear finite element analysis model based on the experimental model is shown in Figure 3(c). Both the concrete and steel impacting cars adopted hexahedral elements with single integral points, and the reinforcement elements adopted Hughes-Liu sectional integral beams of 2 3 2 Gauss integral elements. Also, both the longitudinal reinforcements and the stirrups were regarded as elastic-plastic materials, which could be reasonably described using a piecewise nonlinear model. In this study, the dynamic intensification factor (DIF) rela- tionships provided by Li and Hao28 were used to con- sider the strain rate effects. The relationships between the strain rates and DIF were obtained using equation

(17). The model was described using multi-stage elastic- plastic curves. In the current investigation, DIF = 1 represented the material state description under the quasi-static conditions. The corresponding yield point could then be expressed as the material changes from an elastic state to a plastic state when the stress level reached 350 MP and the strain reached 0.2%. As shown in Figure 3(b), the superstructure in the experi- ments was an axial hydraulic loading platform, and the keyword named *LOAD_BODY_Z was used in the numerical model in order to apply the gravity load to the entire model, and was equivalently simplified with an elastic material of suitable mass. The mass of the elastic material could be adjusted by changing its thick- ness. Similarly, due to the fact that the stiffness of the RC structure was far less than that of the steel trolley, the steel trolley was simplified as an elastic material for calculation purposes. Table 6 details the material parameters:

$$\mathrm{DIF}_s = \left(\frac{\dot{\varepsilon}}{10^{-4}}\right)^{0.074-0.040\frac{f_y}{414}} \qquad (17)$$

In the current study, LS-DYNA contact keyword *CONTACT_SURFACE TO SURFACE contact algo- rithm was used between the mass object and column, and the keyword named *CONTROL_DYNAMIC_ RELAXATION was used for the dynamic relaxation analysis of the structure 0.1 s prior to the calculation in

ISSN 2319-5991 www.ijerst.com

Vol. 14, Issue 4, 2018

Table 6. Model material parameters.

Type	Material modal	Parameter	Magnitude
Longitudinal rebar	PIECEWISE_LINEAR_PLASTICITY (*MAT_024)	Mass density	7850 kg/m^3
		Modulus of elasticity	205,000 Mpa
		Poisson's ratio	0.3
		Yield stress	400 MPa
		Failure strain	0.4
Stirrup	PIECEWISE_LINEAR_PLASTICITY (*MAT_024)	Density	7850 kg/m^3
		Modulus of elasticity	205,000 Mpa
		Poisson's ratio	0.3
		Yield stress	335 MPa
		Failure strain	0.4
Steel plates, Steel impactor	ELASTIC (*MAT_03)	Mass density	7850 kg/m^3
		Modulus of elasticity	205,000 Mpa
		Poisson's ratio	0.3
Concrete	CSC Modal (*MAT_159)[22]	Mass density	2490 kg/m^3
		Compressive strength	42 MPa
		Maximum aggregate size	15 mm
		EROD	1.1
		RECOV	10.4

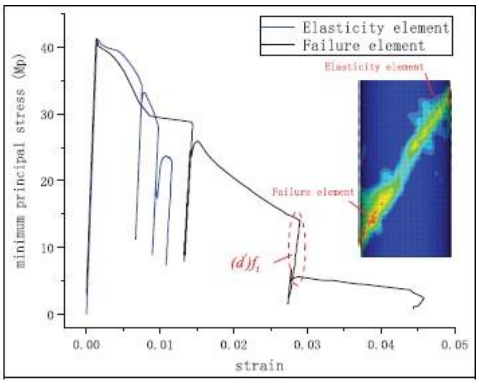

Figure 9. Cylinder model and result diagram.

order to ensure the stability of the axial force applica- tion. Then, based on the research results obtained by Yuan et al.29 regarding grid size sensitivity, the concrete grid size was controlled at 10 mm. In addition, since the deformations of the steel impact trolley were very small during the contact processes, it could be regarded as a rigid body. Therefore, its grid was divided into 50 mm. In regard to the contact setting between the reinforce- ment and the concrete, CONSTRAIN_BEAM IN SOLID was used to consider the slip effects between the reinforced concrete.

Concrete material model validation

The key validity proof CSC modal in that the plastic deformation is determined whether it can be reasonably and unloading stress occurs reasonable. This section refers to the simple finite element model of F150*300 mm cylinder proposed by Malvar,30 as shown in Figure 9. The axial compression experiments of the cylinders were simulated and cyclic loading was carried out through a displacement process. The mate- rial parameter settings were described in a previous sec- tion. As shown in Figure 9, the stress–strain development process of the elastic element and the fail- ure element during the loading process were recorded, respectively, and compared with the experimental and finite element model results in literature,31,32 the model was able to accurately reflect the effects of stiffness degradation during the damage accumulation pro- cesses. Similarly, trial calculations of the concrete con- stitutive model were conducted using the established experimental model. Figure 10 shows the impact force time history and crack development of Component C4 measured in the experiment, and the experimental results were compared with the numerical calculation results. The results showed that the constitutive model was able to reasonably predict the peak value of the impact force and the development of impact force under low velocity impact conditions. The differences between the calculated results and the experimental results were determined to be less than 10%.

Modal analysis of damaged model

Due to the oblique punching cracks (Figure 10) which occurred after impact, pre-existing damages were required in the numerical calculations. The pre-existing damage (PRED) parameters provided by the CSC model reasonably solved this issue. Modal analysis was

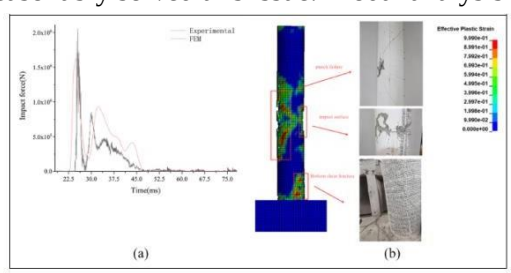

Figure 10. Experimental results of Component C4 and comparison of the value calculation results: (a) dynamic responses of specimens C4 and (b) impact damage of specimens C4.

Table 7. Comparison of the modal frequencies under different damage degrees.

Model frequencies/ PRED	0	0.1	0.3	0.5	0.7
1st	22.3851	21.57	19.67	17.50	15.57
2nd	98.4437	94.48	85.58	75.70	63.98
3nd	230.4552	217.99	192.20	162.93	126.98

ISSN 2319-5991 www.ijerst.com

Vol. 14, Issue 4, 2018

carried out for the same calculation model under differ- ent PRED values, and the results are shown in Table 7. It was found that the increases in the PRED values led to nonlinear reductions of the modal frequencies.

Restart technology provides the possibility to study the cumulative damage problems of RC piers and modal analysis. Kishi et al.33 carried out experiments and numerical simulations of these problems. However, the method provided by KISHI was only applicable to the problems related to the impacts between simple rigid bodies, and was not applicable to nonlinear large deformation impact problems with complex structures and many failure factors. Therefore, this study pro- vided a new restart method as follows:

1. Following the first calculation, the calculation results were checked using the post-processing software Ls-Prepost, and the experimental data were compared. When the calculation results were found to be correct, the OUTPUT option in Ls-Prepost was used to output such data as the element and nodes, in order to use these data in a geometric model for the next calculation.

2. At the same time, the stress and plastic strain of all the elements at the completion of the first calculation were output through DYNAIN option in Ls-Prepost, and the initial damages were applied to the material for the purpose of forming a stress-strain initialization file at the initial time of the second calculation.

3. Then, the solution options and assemble a geo- metry file and stress initialization file were reset in order to obtain the second impact file. It was worth noting that the model could be appropri- ately simplified during the assembly of the modal analysis files, such as removing the steel trolley and the upper steel plate, as well as set- ting the solver to implicit analysis.

In the current investigation, in order to ensure the accuracy of the modal calculations, the PRED values were adjusted in order to ensure that the MAC values

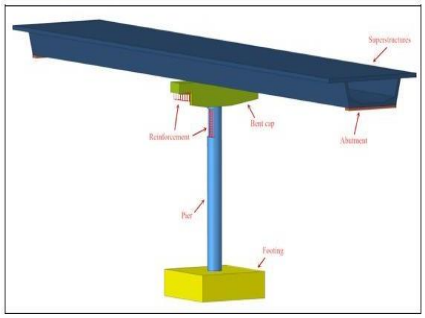

Figure 11. Specific sizes of the pier models.

were within a reasonable range. Then, the range was divided in order to facilitate the calculation process. Table 7 shows the numerical calculated modal frequency values. The results show that the calculation method is suitable for the present study.

Vehicle-bridge impact model

The DCI can also provide references for engineering designs. In order to study the relationships between dynamic responses and modal frequencies of bridge piers under the effects of cumulative impacts of vehi- cles, a large number of numerical simulation calcula- tions were carried out using columns with different section sizes, and various impact velocities and vehicle masses. The results showed that there were two types of impact forces at the time of impact, which were con- trolled by the cargo mass and velocity values. It was found that according to the experimental results, the appropriate finite element analysis parameters could be determined. Then, when combined with the Ford F800 medium truck model developed by National Crash Analysis Center (NACA) and a full-scale model of the pier to verify the validity of DCI damage indicators used in this study. Through regression analysis, the rela- tionship between damage degree and dynamic response was studied.

Information regarding the piers and vehicles

In order to ensure the validity of the finite element model, this study adopted the same modeling method as described in Section ‘‘Concrete material model vali- dation,’’ including the material model, contact mode, and strain rate effect parameters. Consolazio et al. proposed that a bridge model composed of a

ISSN 2319-5991 www.ijerst.com

Vol. 14, Issue 4, 2018

bridge columns and two spans can effectively predict the dynamic response of a multi-span bridge, and the prototype problem had been simplified which consists of a circular single column, superstructure and two supports. As shown in Figure 11, the size of 5000 mm 3 5000 mm 3 1200 mm the concrete foundation was to place a trapezoidal solid beam on the top of the column to transmit the weight of the superstructure with a length of 30 m to the pier column. Its weight changed with the size of the column section to ensure that all collision scenarios maintain the same axial com- pression ratio. All collision cases are shown in Table 8. The superstructure of the bridge pier was connected to the column by rubber bearings. Previously research by EI-TAWIL et al. had shown that the stiffness of the sup- port has a negligible effect on the overall dynamic response of the pier. Here it is assumed that the vertical portion of the pier by contacting the concrete surface, using the LS-DYNA keyword named CONTACT AUTOMATIC SURFACE TO SURFACE.

As shown in Figure 12, the Ford vehicle model was used to represent the collision of the vehicle on the bridge pier, Abdelkarim et al.11 and Sharma et al.21 shared the model and verified its accuracy through experimental tests. In this study's model, the total mass of the Ford truck was 8 t, including a 0.24 t engine mass and a 2.8 t cargo mass. The engine and cargo were simulated using elastic materials, with an elastic modu- lus of 11,000 MP and 2000 MP. The weight of the vehicle model was controlled by changing the quality of the goods.

Vehicle impact responses

Peak impact force (PIF). The change of damage degree is reflected by cumulative impact.. The typical time

Table 8. Numerical simulations of the component information.

scenarios	Column size (mm)	Longitudinal reinforcement ratio ρ_0 (%)	Hoop reinforcement ratio ρ_v (%)	Axial compression ratio ρ_n (%)
C800-V60-W8 C800-V90-W8 C800-V110-W8	800	10C22 (0.756)	25@150 mm (1.31)	388 t (40.5)
C1000-V60-W8 C1000-V90-W8 C1000-V110-W8	1000	10C28 (0.784)	25@150 mm (1.08)	612.95 t (40.5)
C1200-V60-W8 C1200-V90-W8 C1200-V110-W8 C1200-V60-W10 C1200-V90-W10 C1200-V110-W10 C1200-V60-W12 C1200-V90-W12 C1200-V110-W12	1200	10C32 (0.711)	25@150 mm (0.95)	859.6 t (40.5)

In the table, C800-V60-W8-1 indicates that the 800 mm diameter column is the first to be impacted by the vehicles with a total weight of 8 t and a speed of 60 km/h; 10C22 means 10 steel bars with a diameter of 22 mm; 25@150 means that the stirrup spacing is 150 mm and the diameter is 25 mm.

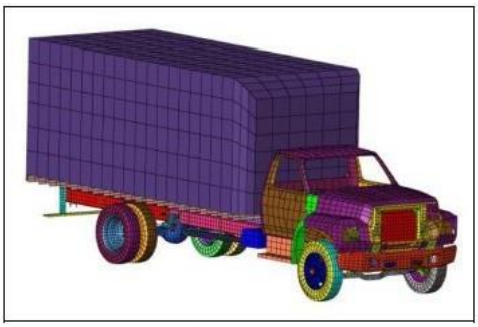

Figure 12. Truck model.

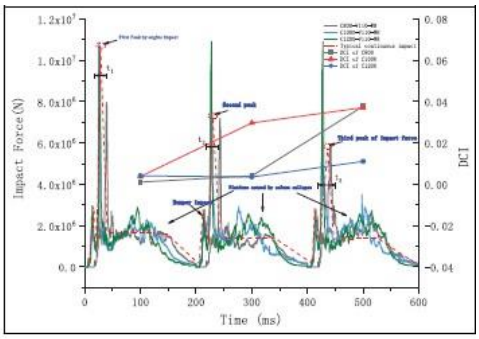

Figure 13. Time history diagram of the typical continuous impact force and damage degrees of the bridge piers.

history of the three consecutive impacts and corre- sponding DCI values are shown in Figure 13. In the fig- ure, a time history diagram of the three impact forces (C800/1000/1200) of the V110-W8 component is detailed. Each calculation time was set as 200 ms, with 400 ms being the end time of the second impact and the beginning time of the third impact, respectively. The peak values of the three impact forces were all caused by the contact between the engine and the bridge pier. Therefore, according to the comparison results, the time history diagram of the first typical impact force was consistent with the form of the time history dia- gram of the impact force developed by Chen et al.34 and Cao et al.35 Figure 14 describes the damage degrees of the components using the effective plastic strain after impact. The accumulation of the impact times caused the modal parameters of the components to gradually move away from their initial states, and the decreases in the stiffness values led to decreases in the PIF values. This phenomenon was found to be representative of piers which had suffered accidents. It was also worth noting that this

ISSN 2319-5991 www.ijerst.com

Vol. 14, Issue 4, 2018

phenomenon was not obvious in C1200-V110-W8. This was due to the fact that the impacting effects of the medium-sized truck at that speed had difficulty affecting the stiffness values of the pier of that particular size. As shown in Figures 13 and 14, results show that DCI values with increasing degree of damage increases. For a stronger ability to resist piers, which rise in value more slowly degree, demon- strate the effectiveness of DCI pier damage detection.

Table 9 details the statistical data of the numerical simulation results of the columns with different sizes, including the peak values, duration Tn, and 25 ms

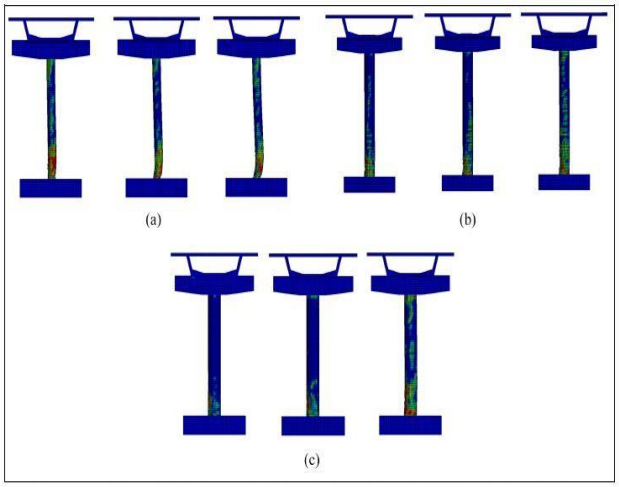

Figure 14. Comparison of the impact damage degrees: (a) C800-V110-W8, (b) C1000-V110-W8, and (c) C1200-V110-W8.

Table 9. Numerical simulation results.

Scenarios	First impact			Second impact			Third impact		
	PIF (MN)	ESF (MN)	DCI	PIF	ESF	DCI	PIF	ESF	DCI
C800-V60-W8	2.27	1.510	0.00033	2.52	1.546	0.00546	2.4	1.537	0.00736
C800-V90-W8	7.08	2.069	0.00060	6.35	2.131	0.01363	7.16	2.092	0.02769
C800-V110-W8	9.88	2.175	0.00105	7.86	2.526	0.01641	5.85	2.752	0.03779
C1000-V60-W8	2.12	1.450	0.00028	2.22	1.494	0.00058	2.13	1.530	0.00104
C1000-V90-W8	8.2	2.314	0.00069	6.73	2.337	0.00186	7.06	2.225	0.01035
C1000-V110-W8	10.9	2.423	0.00379	7.85	2.852	0.02971	6.38	2.714	0.03709
C1200-V60-W8	3.01	1.621	0.00019	3.23	1.634	0.01150	2.75	1.507	0.02445
C1200-V90-W8	8.89	2.224	0.00054	8.16	2.106	0.00103	6.4	2.178	0.00901
C1200-V110-W8	10.7	2.549	0.00411	10.7	2.532	0.00355	7.93	2.533	0.01107
C1200-V60-W10	3.07	1.601	0.00004	2.62	1.537	0.00121	2.70	1.554	0.00335
C1200-V90-W10	8.01	2.374	0.00025	6.08	2.350	0.00177	7.85	2.428	0.01308
C1200-V110-W10	11.9	2.523	0.00749	8.89	2.687	0.014437	8.39	2.428	0.02547
C1200-V60-W12	3.14	1.595	0.00029	2.57	1.549	0.002741	2.95	1.563	0.01451
C1200-V90-W12	8.14	2.253	0.00643	7.34	2.297	0.017594	4.37	2.181	0.02314
C1200-V110-W12	12.20	2.553	0.00314	6.39	2.731	0.019881	6.32	2.662	0.02495

equivalent static calculation results of each impact force. All of the components in the table were impacted by a medium-sized vehicle of 8 t, which represented a typical type of engine impact scenario.

The studies conducted by EI-TAWIL [40] showed that the peak force formula (equation (18)) of ship- bridge impacts provided by American Association of State Highway and Transportation Officials (AASHTO) was also applicable to vehicle impacts. The impact velocity V (m/s) and the mass W (kg) of the impacting bodies were considered in the formula. In this study, a new expression equation (20) was pro- posed for the pre-damaged impact problem, and two dimensionless parameters, damage factor DCI, and the

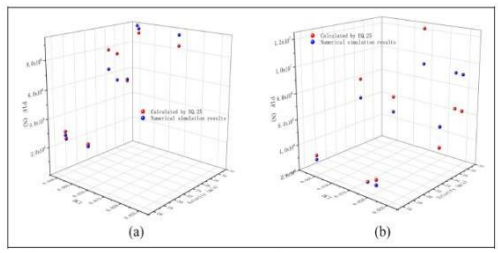

Figure 15. Comparison between simulation results and equation (20): (a) C1200-W10 and (b) C1200-W12.

equivalent stiffness (b/800) were introduced. Therefore, the formula was able to achieve a more comprehensive description of each parameter. Five regression coeffi- cients (referred to as a, b, c, d, and e) were determined using a nonlinear regression analysis method. It was found that when subjected to continuous impacts, the PIF engine could be estimated using equation (20). Figure 15 details this study's comparison of the fitting results and the numerical simulation results

$$F_i = f\{\alpha(V)^{\beta}(W)^{\gamma}\} \quad (18)$$

$$\mathrm{PIF} = f\left\{a(DCI)^{b}(V)^{c}(W)^{d}\left(\frac{b}{800}\right)^{e}\right\} \quad (19)$$

$$\mathrm{PIF}_{\mathrm{engine}} = 10027.08(DCI)^{-0.044}(V)^{2.13}(W)^{-0.085}\left(\frac{b}{800}\right)^{0.364} \quad (20)$$

5. Conclusion

The frequency domain-based correlation technique (DCI), proposed in this work, was applied to identify damage and assess the structural safety of the bridge piers affected by low-speed vehicles. Its practicality and application were verified. The following conclusions were drawn from the study's findings:

1. The fast Fourier transform (FRFs) processing was used to obtain the modal frequency parameters of the structures, and the measurements of the frequency response functions of the structures with impact damages were the main techniques in the recommended procedure. It was found that the cracking

ISSN 2319-5991 www.ijerst.com

Vol. 14, Issue 4, 2018

processes had a major effect on the columns' inherent frequencies. Moreover, the impacts resulted in nonmonotonic reductions in the modal frequencies and a decrease in the stiffness values of the columns at the crack sections. As a result, the gathered data may be used to compute and compare the structural damage correlation indexes (DCI). The results demonstrated that the DCI could predict residual stiffness values and the degree of structural damage with accuracy.

2. The accuracy of the benchmark experimental model is validated, and the finite element approach-based calculation techniques for modal identification following structural damage and impact on reinforced concrete columns are introduced.

3. The current study inquiry used a finite element method to compute the predamaged vehicle-pier impact events. Using the DCI, equation (20) was utilized to predict the highest impact force. Comparing the proposed formula to the conclusions drawn from similar research initiatives, it was shown to have the advantage of taking into account the reductions in impact force and the loss of stiffness caused by structural defects. Consequently, the proposed method provided a helpful starting point for further structural design phases.

References

1. Cook W, Barr PJ and Halling MW. Bridge failure rate. J Perform Constr Facil 2015; 29: 04014080.

2. Gomes GF, Mende´z YAD, Alexandrino PSL, et al. The use of intelligent computational tools for damage detec- tion and identification with an emphasis on composites: a review. Compos Struct 2018; 196: 44–54.

3. Perez MA, Gil L and Oller S. Impact damage identifica- tion in composite laminates using vibration testing. Com- pos Struct 2014; 108: 267-276.

4. Zenzen R, Belaidi I, Khatir S, et al. A damage identifica- tion technique for beam-like and truss structures based on FRF and Bat algorithm. CR Me´canique 2018; 346: 1253–1266.

5. Liu S, Zhang L, Chen Z, et al. Mode-specific damage identification method for reinforced concrete beams: con- cept, theory and experiments. Constr Build Mater 2016; 124: 1090–1099.

6. Sha G, Cao M, Radzien´ski M, et al. Delamination- induced relative natural frequency change curve and its use for delamination localization in laminated composite beams. Compos Struct 2019; 230: 111501.

7. Sampaio RPC, Silva TAN, Maia NMM, et al. Damage identification based on response functions in time and frequency domains. In: Nobari AS and Ferri Aliabadi MH (eds) Vibration-based techniques for damage detection and localization in engineering structures. China: World Scientific Publishing Co Pte Ltd, 2018, pp. 197–236.

8. Pe´rez MA, Pernas-Sa´nchez J, Artero-Guerrero JA, et al. High-velocity ice impact damage quantification in com- posite laminates using a frequency domain-based correla- tion approach. Mech Syst Signal Process 2021; 147: 107124.

9. Officials AAoSHaT. AASHTO-LRFD. Bridge design specifications – customary US Units. 5th ed. Washington, DC: Officials AaoSHaT, 2010.

10. Chen L, El-Tawil S and Xiao Y. Reduced models for simulating collisions between trucks and bridge piers. J Bridge Eng 2016; 21: 04016020.

ISSN 2319-5991 www.ijerst.com

Vol. 14, Issue 4, 2018

11. Abdelkarim OI and ElGawady MA. Performance of bridge piers under vehicle collision. Eng Struct 2017; 140:337–352.

12. Al-Thairy H and Wang YC. An assessment of the current Eurocode 1 design methods for building structure steel columns under vehicle impact. J Constr Steel Res 2013; 88: 164–171.

13. Buth CE, Brackin MS, Williams WF, et al. Collision loads on bridge piers: phase 2, report of guidelines for designing bridge piers and abutments for vehicle collisions. Bryan, TX: Texas Transportation Institute, 2011.

14. Buth CE, Williams WF, Brackin MS, et al. Analysis of large truck collisions with bridge piers: phase 1, report of guidelines for designing bridge piers and abutments for vehicle collisions. Bryan, TX: Texas Transportation Insti- tute, 2010.

15. Chen L, Xiao Y, Xiao G, et al. Test and numerical simu- lation of truck collision with anti-ram bollards. Int J Impact Eng 2015; 75: 30–39.

16. Cai J, Ye JB, Chen QJ, et al. Dynamic behaviour of axially-loaded RC columns under horizontal impact loading. Eng Struct 2018; 168: 684–697.

17. Zhou XW, Zhou M, Gao YS, et al. An evaluation study on the cumulative impact damages of reinforced concrete piers based on modal frequencies. Eng Fail Anal 2021; 119: 104983.

18. Adhikary SD, Li B and Fujikake K. Dynamic behavior of reinforced concrete beams under varying rates of con- centrated loading. Int J Impact Eng 2012; 47: 24–38.

19. Pham TM and Hao H. Influence of global stiffness and equivalent model on prediction of impact response of RC beams. Int J Impact Eng 2018; 113: 88–97.

20. Chen L, Wu H and Liu T. Shear performance evaluation of reinforced concrete piers subjected to vehicle collision. J Struct Eng 2020; 146: 04020026.

21. Sharma H, Hurlebaus S and Gardoni P. Performance- based response evaluation of reinforced concrete columns subject to vehicle impact. Int J Impact Eng. 2012; 43: 52–62.

22. Murray YD. Users manual for LS-DYNA concrete material model 159. No. FHWA-HRT-05-062. Washing- ton, DC: United States Federal Highway Administration Office of Research, Development, and Technology, 2007.

23. Pastor M, Binda M and Harcˇarik T. Modal assurance cri- terion. Procedia Eng 2012; 48: 543–548.

24. Allemang RJ. The modal assurance criterion – twenty years of use and abuse. Sound Vib 2003; 37: 14–23.

25. Ahlgren P, Jarneving B and Rousseau R. Requirements for a cocitation similarity measure, with special reference to Pearson's correlation coefficient. J Am Soc Inform Sci Technol 2003; 54: 550–560.